Progress In Electromagnetics Research, PIER 101, 349–374, 2010

AN INNOVATIVE MULTI-SOURCE STRATEGY FOR ENHANCING THE RECONSTRUCTION CAPABILITIES OF INVERSE SCATTERING TECHNIQUES

F. Caramanica and G. Oliveri

Department of Information and Communication Technology
University of Trento-Via Sommarive
Trento 14-38050, Italy

Abstract—Active microwave imaging techniques are aimed at reconstructing an unknown region under test by means of suitable inversion algorithms starting from the measurement of the scattered electromagnetic field. Within such a framework, this paper focuses on an innovative strategy that fully exploits the information arising from the illumination of the investigation domain with different configurations as well as radiation patterns of the probing sources. The proposed approach can be easily integrated with multiview techniques and, unlike multifrequency methods, it does not require additive *a-priori* information on the dielectric nature of the scatterer under test. A large number of numerical simulations concerned with 2D geometries confirms the effectiveness of the inversion strategy as well as its robustness with respect to noise on data. Moreover, the results of a comparative study with single-source methodologies further point out the advantages and potentialities of the new approach.

1. INTRODUCTION

In the last years, the scientific community has addressed a growing interest to the detection and imaging of unknown objects located in inaccessible domains by means of electromagnetic fields at microwave frequencies. As a matter of fact, the propagation of an electromagnetic wave in the microwave range is significantly affected by the characteristics of the medium. Therefore, it is profitable to exploit such a phenomenon in order to sense an unknown scenario in a non-invasive fashion. Towards this end, several researches have

Corresponding author: G. Oliveri (giacomo.oliveri@disi.unitn.it).

been pursued in the framework of subsurface monitoring [1, 2], non-destructive evaluation and testing [3, 4], and biomedical diagnostics [5–7].

Whatever the application, a microwave imaging setup consists of a probing source that senses an inaccessible investigation domain and a set of receivers collecting samples of the electromagnetic field scattered by the structure under test. After the measurement phase, a post-processing of the collected data is performed to provide a faithful reconstruction of the scenario under test. Such a retrieval process presents some intrinsic drawbacks [8, 9], which make the inversion of the scattering data hard to cope with. Firstly, if a complete and quantitative reconstruction of the electromagnetic properties is desired, multiple scattering effects cannot be neglected and a full non-linear model should be considered. Moreover, the ill-posedness and the ill-conditioning of the problem [10] are key-issues to be carefully addressed. They are due to the lack of information coming from measured scattering data. During the imaging process, a huge amount of parameters has to be retrieved starting from a limited number of independent measurements. Thus, if neither *a-priori* information are available nor other physical constraints are imposed, there is the need to collect other information by means of suitable techniques besides the use of effective retrieval techniques [11–15].

Within such a framework, different strategies aimed at increasing the information content of scattering data have been proposed in the related literature. Let us consider the multi-view strategy proposed in [16] where the scatterer is illuminated from different angular directions in order to give an "overview" of the scenario under test. As determined in [17], such a technique allows a significant increasing of independent scattering data with respect to single-view experiments. However, even though a multiview method can partly add information, it cannot fully overcome the substantial lack of information.

Another widely-used countermeasure resorts to a multi-frequency approach [18–21] or a frequency-hopping scheme [22]. As far as the collectable information is concerned, the number of independent data certainly increases since different and complementary scattering effects are excited by a set of incident electromagnetic fields at different frequencies. However, to fully exploit such an enhancement of the knowledge on the scenario at hand, some *a-priori* assumptions have to be done about the dispersion model of the dielectric characteristics of the scatterer [19].

The "informative content" has been also enhanced by exploiting the so-called *acquired information* during the inversion [23, 24] or using different polarizations [25–28].

In this paper, an innovative methodology aimed at increasing the amount of scattering data (avoiding further *a-priori* assumptions on the investigation domain) is proposed. The multi-source (MS) approach supposes the investigation domain illuminated by different probing sources, each of them with a proper (and different) radiation pattern, to induce different scattering interactions able to "show" different "aspects" of the scatterer under test. Integrated with a multi-view strategy, the exploitation of the "source diversity" (through the definition of a suitable multi-source/multi-view cost function) enlarges in a non-negligible fashion the number of retrievable unknowns by enhancing the robustness of the imaging process against the noise and the stability of the inversion procedure as well as the reconstruction accuracy. The arising reduction of the ratio between dimension of the space of the unknowns and that of data also implies a decreased sensitivity to false solutions [29] leading to a more tractable optimization problem.

In the following, after the mathematical formulation of inverse scattering interactions arising in the microwave imaging process, the multi-source technique is introduced and described (Section 2). Section 3 is devoted to the numerical assessment of the effectiveness and robustness of the proposed strategy. Towards this aim, selected numerical experiments concerned with layered as well as complex scatterers will be discussed. To point out the enhanced reconstruction accuracy, the results of a comparative study will be presented and analyzed. Finally, some conclusions will be drawn (Section 4).

2. MATHEMATICAL FORMULATION

Let us consider a two-dimensional scenario for microwave imaging of cylindrical bodies, $\hat{\mathbf{z}}$ being the symmetry axis. With reference to Fig. 1, the electromagnetic properties of the investigation domain D_I are described through the unknown contrast function $\tau(x,y) = \varepsilon_r(x,y) - 1 - j\frac{\sigma(x,y)}{2\pi f \varepsilon_0}$, $(x,y) \in D_I$ where $\varepsilon_r(x,y)$ is the relative dielectric permittivity, ε_0 the free-space permittivity, f is the frequency, and $\sigma(x,y)$ is the conductivity. The background is known and it is assumed to be homogeneous and characterized by τ_0.

To image the scenario under test and reconstruct the dielectric profile $\tau(x,y)$, the investigation region is sensed with S electromagnetic sources radiating different beampatterns. Moreover, each source successively probes D_I from V different angular positions θ^v according to a multi-view approach [16]. The radiated incident electric field is denoted by $E_{inc}^{v,s}(x,y)\hat{\mathbf{z}}$, $v = 1,\ldots,V$, $s = 1,\ldots,S$.

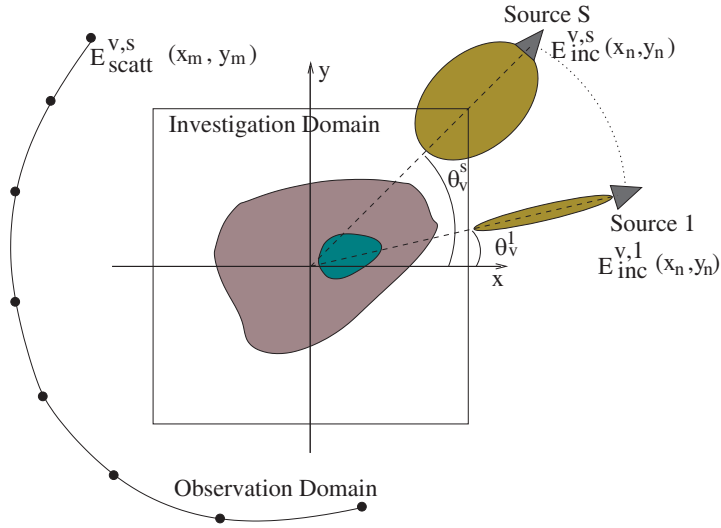

Figure 1. Geometry of the multi-source/multi-view imaging system.

The effects of the interactions between incident fields and scatterers are revealed by collecting a set of measurements of the scattered electric field. At each sensor located within the observation domain D_O, the following set of samples is available: $E^{v,s}_{scatt}(x^v_m, y^v_m)\hat{\mathbf{z}}$, $v = 1, \ldots, V$, $m^v = 1, \ldots, M^v$, $s = 1, \ldots, S$. Analytically, the relation between scatterers and diffused field can be expressed through the integral "*Data*" equation [8]

$$E^{v,s}_{scatt}(x^v_m, y^v_m) = j\frac{k_0^2}{4}\int_{D_I} \tau(x', y') E^{v,s}_{tot}(x', y') G_{2D}(x^v_m, y^v_m \,|x', y')dx'dy' \qquad (x^v_m, y^v_m) \in D_O \quad (1)$$

where k_0 is the background wavenumber and G_{2D} is the two-dimensional free-space Green's function [30]. Analogously, the known incident field $E^{v,s}_{inc}(x, y)\hat{\mathbf{z}}$ in D_I is related to the scatterers properties as follows ("*State*" integral equation)

$$E^{v,s}_{inc}(x, y) = E^{v,s}_{tot}(x, y) - j\frac{k_0^2}{4}\int_{D_I} \tau(x', y') E^{v,s}_{tot}(x', y') G_{2D}(x, y|x', y')dx'dy' \qquad (x, y) \in D_I \quad (2)$$

Unfortunately, such a description is mathematically tractable only after a suitable discretization. According to the Richmond's

procedure [31], by considering N rectangular basis function

$$\Omega_n(x,y) = \begin{cases} 1 & (x,y) \in D_I^{(n)} \\ 0 & (x,y) \notin D_I^{(n)} \end{cases} \tag{3}$$

($D_I^{(n)}$ being the n-th partition of the investigation domain), the reconstruction process moves towards the retrieval of the discretized representation of the unknowns

$$\tau(x,y) = \sum_{n=1}^{N} \tau_n \Omega_n(x,y) \qquad E_{tot}^{v,s}(x,y) = \sum_{n=1}^{N} E_n^{v,s} \Omega_n(x,y).$$

Thus, the problem unknowns turn out to be τ_n, $E_n^{v,s}$, $n = 1,\ldots,N$, $v = 1,\ldots,V$, $s = 1,\ldots,S$. The number of the expansion coefficients defines the dimension of the unknown-space U. Typical drawbacks of the inverse scattering problem at hand are its ill-posedness and the ill-conditioning [10], both due to the limited amount of the available and collectable information, that make the inversion of scattering data instable and inaccurate without proper countermeasures. Consequently, the inverse problem has to be carefully managed by properly defining a least-square solution and a suitable regularization strategy. Towards this end, a widely adopted technique consists in imposing a set of constraints related to inverse scattering data or to the *a-priori* knowledge to be satisfied in a least-square fashion by minimizing a suitable cost function.

It is well known that to come to a well-posed and well-conditioned problem, a necessary condition (although not sufficient) is that U be less than the essential dimension of the scattering data I or the number of arising independent constraints[†]. Therefore, managing scattering data (and corresponding constraints) as well as the exploitation of *a-priori* information is a key issue, since it strongly affects the overall inversion procedure and the possibility of obtaining a faithful reconstruction of the actual profile. To effectively address such an issue, an innovative approach that fully exploits scattering data from a multi-source system is formulated in the following.

Let us consider a standard multi-view arrangement where the s-th source probes the investigation domain. As far as the fitting with the arising scattering data [$E_{scatt}^{s,v}(x_m^v, y_m^v)$ and $E_{inc}^{s,v}(x_n, y_n)$] is concerned,

[†] In fact, each linear constraint can be equivalently seen as a reduction of the number of independent unknowns.

the solution is requested to satisfy the following constraints

$$\begin{aligned}\phi^{(s)}_{Data}\left\{\tau_n, E^{v,s}_n\right\} &= \frac{C^{(s)}_{Data}\left\{\tau_n, E^{v,s}_n\right\}}{c^{(s)}_{Data}} = 0\\ \phi^{(s)}_{State}\left\{\tau_n, E^{v,s}_n\right\} &= \frac{C^{(s)}_{State}\left\{\tau_n, E^{v,s}_n\right\}}{c^{(s)}_{State}} = 0\end{aligned} \tag{4}$$

$$\begin{aligned}&C^{(s)}_{Data}\left\{\tau_n, E^{v,s}_n\right\}\\ &= \sum_{v=1}^{V}\sum_{m^v=1}^{M^v}\left|E^{s,v}_{scatt}(x^v_m, y^v_m) - \sum_{n=1}^{N}\tau_n E^{v,s}_n G^v_{2D}(x^v_m, y^v_m\,|x_n, y_n)\right|^2\end{aligned} \tag{5}$$

$$\begin{aligned}&C^{(s)}_{State}\left\{\tau_n, E^{v,s}_n\right\}\\ &= \sum_{v=1}^{V}\sum_{n=1}^{N}\left|E^{s,v}_{inc}(x_n, y_n) - \left[E^{v,s}_n - \sum_{p=1}^{N}\tau_p E^{v,s}_p G^v_{2D}(x_n, y_n|x_p, y_p)\right]\right|^2\end{aligned} \tag{6}$$

where

$$c^{(s)}_{data} = \sum_{v=1}^{V}\sum_{m^v=1}^{M^v}\left|E^{s,v}_{scatt}(x^v_m, y^v_m)\right|^2,\ c^{(s)}_{State} = \sum_{v=1}^{V}\sum_{n=1}^{N}\left|E^{s,v}_{inc}(x_n, y_n)\right|^2,$$

and

$$\begin{aligned}&G^v_{2D}(x_r, y_r|x_t, y_t)\\ &= \begin{cases}(j/2)\left[\pi k_0 a_r H^{(2)}_0(k_0 a_r) - 2j\right] & \text{if } r = t \text{ and } (x_r, y_r) \in D_I\\ (j\pi k_0 a_r/2) H^{(1)}_0(k_0\rho^v_{rt}) J_1(k_0 a_r) & \text{if } r \neq t \text{ or } (x_r, y_r) \notin D_I\end{cases}\end{aligned} \tag{7}$$

$\rho^v_{rt} = \sqrt{(x^v_r - x_t)^2 + (y^v_r - y_t)^2}$; $H^{(2)}_0(\,.\,)$ and $H^{(1)}_0(\,.\,)$ are the first and second kind 0-*th* order Hankel function, respectively; $J_1(\,.\,)$ is the Bessel function; $k_0 = \frac{2\pi}{\lambda_0}$ (λ_0 being the background wavelength) and $a_r = \sqrt{\frac{A^{(n)}_I}{\pi}}$, $A^{(n)}_I$ being the area of $D^{(n)}_I$.

Because of the properties of the scattered field, the amount of independent information arising from such a (s-th) multi-view experiment (and collectable from the $\sum_{v=1}^{V} M^v$ measurements in D_O) is not larger than a fixed threshold I [17]. Therefore, the solution $\{\tau_n, E^{v,s}_n\}$ that best fits (4) cannot be faithfully retrieved without reducing the spatial resolution accuracy N until U is lower than such a threshold.

As a matter of fact, the information related to a single-source (SS) multi-view experiment might be insufficient to guarantee satisfactory

reconstructions and different strategies have to be investigated to increase the information content of scattering data. A widely adopted technique is the so-called multi-frequency approach [18–20] that certainly can improve the reconstruction accuracy of the imaging process by increasing the number of independent data, but generally it requires some assumptions on the dielectric properties of the scenario under test. Indeed, even though the object function does not change when changing the source-position (or illumination), it varies with frequency. Thus, without some *a-priori* information, the solution of different inverse scattering problems is necessary with a large increasing of the computational load and computer memory requirements.

Within the same framework, the multi-source technique also is aimed at enlarging the amount of informative scattering-data in order to enhance the reconstruction accuracy. However, while the contrast function of the multi-frequency approach is a function of the frequency $[\tau_n \sim \tau_n(f)]$, in such a case, the unknown coefficients τ_n are independent on the source model $[\tau_n \nsim \tau_n(s)]$. The underlying idea of the multi-source approach lies in the assumption (preliminarily verified in [32]) that different electromagnetic sources (with different radiation patterns) might "reveal" different aspects of the object under test since different interactions occur between scatterers and incident fields. Consequently, the measurements of the arising scattered fields allow one to keep different and complementary information that it could be profitable to exploit for improving the accuracy of the imaging process. To fully exploit such information, a suitable combination of the constraints in (4) concerned with each source should be considered. Towards this end, let us define the multi-source cost function Φ_{MS}

$$\Phi_{MS}\{\tau_n, E_n^{v,s}\} = \Phi_{MS}^{Data}\{\tau_n, E_n^{v,s}\} + \Phi_{MS}^{State}\{\tau_n, E_n^{v,s}\} \quad n = 1, \ldots, N;\ v = 1, \ldots, V;\ s = 1, \ldots, S \tag{8}$$

where

$$\Phi_{MS}^{Data}\{\tau_n, E_n^{v,s}\} = \frac{\sum_{s=1}^{S} C_{Data}^{(s)}\{\tau_n, E_n^{v,s}\}}{\sum_{s=1}^{S} c_{Data}^{(s)}} \tag{9}$$

$$\Phi_{MS}^{State}\{\tau_n, E_n^{v,s}\} = \frac{\sum_{s=1}^{S} C_{State}^{(s)}\{\tau_n, E_n^{v,s}\}}{\sum_{s=1}^{S} c_{State}^{(s)}} \tag{10}$$

to be minimized. Towards this end, a deterministic optimizer based on the alternating direction implicit method [33] is used[‡] (see Appendix

[‡] More recent optimization approaches to standard 2D inverse scattering problems developed at the *ELEDIALab* have been described elsewhere [34–36] and their integration, as well as the integration of other state-of-the-art stochastic minimization techniques [37], into the multi-source technique will be a key-issue of future researches.

A) to focus on the effectiveness of the multi-source approach neglecting the "overboost" effects as well as the randomness arising from its integration with a stochastic optimizer (more effective in avoiding the solution is trapped in the local minima of the cost function). More in detail and unlike the modified gradient method, where the unknown fields and contrast are updated simultaneously, but according to the contrast source inversion method [38], $\{[\tau_n]_k;\, n = 1, \ldots, N\}$ and $\{[E_n^{v,s}]_k;\, n = 1, \ldots, N;\, v = 1, \ldots, V;\, s = 1, \ldots, S\}$ are iteratively reconstructed (k being the iteration number) by alternatively updating the two sequences. The minimization algorithm is stopped when a maximum number of iterations, K (i.e., $k \leq K$), or a threshold on the cost function value, δ (i.e., $\Phi_{MS}^{(k)} = \Phi_{MS}\{[\tau_n]_k, [E_n^{v,s}]_k\} \leq \delta$), or the value of the cost function remains unaltered in a fixed percentage of the total amount of the minimization-algorithm iterations (i.e., $\frac{|K_w \Phi_{MS}^{(k)} - \sum_{h=1}^{K_w} \Phi_{MS}^{(h)}|}{\Phi^{(k)}} \leq \varsigma$, K_w being an integer number and ς the threshold on the cost function).

Moreover, to reduce the occurrence of false solutions, the reconstruction approach has been integrated into a multi-resolution methodology (IMSA) [39–41] instead of using a "*bare*" (or *single step*) optimization (ISSA). Such a methodology, which implements a multi-step (i being the step index) synthetic zoom of the region-of-interest (RoI) where the scatterer is estimated, is dependent neither on the minimization approach [23, 42, 43] nor on the imaging system [44, 45] and scattering data [46]. Thus, it can be easily integrated into the multi-source imaging system by enhancing its computational effectiveness.

3. NUMERICAL ANALYSIS

In this section, the effectiveness of the MS approach is evaluated by considering a selected and representative set of numerical experiments.

As a first test case (*Test Case 1*), let us consider the reference profile shown in Fig. 2(a) where a two-dimensional investigation domain of side $L_{D_I} = 3.0\,\lambda_0$ contains a square stratified scatterer $L_{ext} = 0.9\,\lambda_0$-sided centered at $x_c^{ref} = -0.6\,\lambda_0$, $y_c^{ref} = 0.6\,\lambda_0$. The dielectric permittivity of the inner region ($L_{int} = 0.3\,\lambda_0$) is equal to $\varepsilon_r^{int} = 3.0$ ($\tau_{int}(x, y) = 2.0$), while the outer layer has a contrast function $\tau_{ext}(x, y) = 0.5$. Such a configuration has been successively illuminated by $V = 4$ different directions and the measures have been collected at $M^v = 26$, $v = 1, \ldots, V$ equally-spaced points lying on a circular observation domain of radius $r_O = 2.2\,\lambda_0$. The scattering data have been synthetically-generated by considering the following

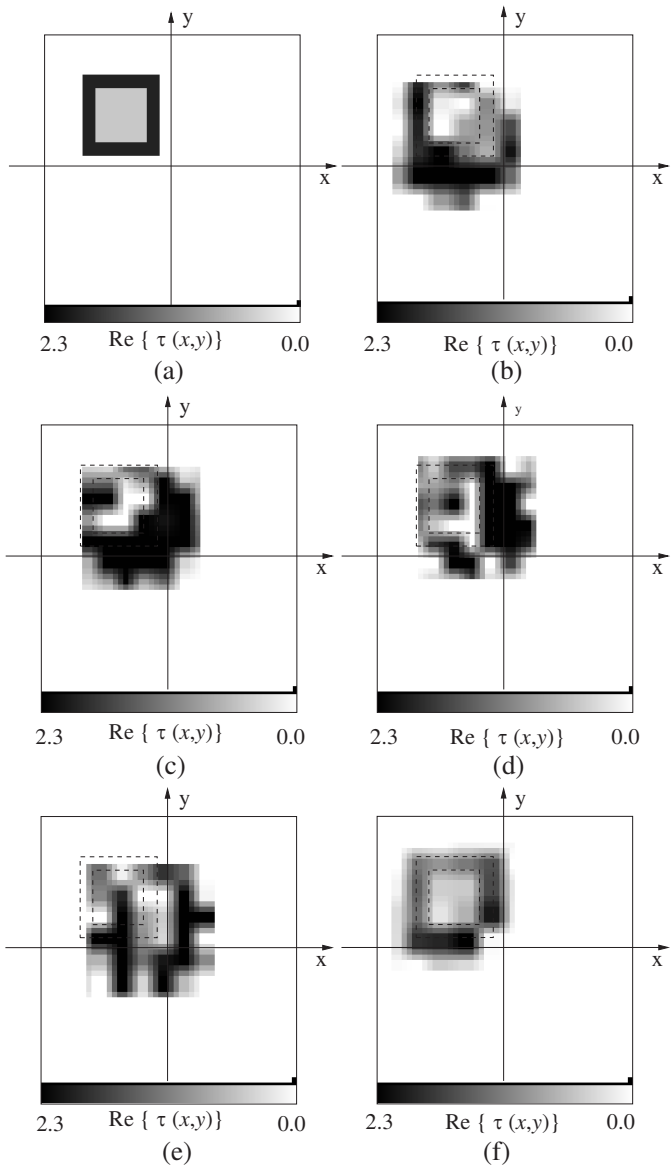

Figure 2. Dielectric profile reconstruction ($\tau_{ext} = 2.0$, $\tau_{int} = 0.5$). (a) Reference distribution. Reconstructed dielectric distribution by using (b) *IMSA-PW*, (c) *IMSA-IL*, (d) *IMSA-DL*, (e) *IMSA-CS*, and (f) *IMSA-MS* ($SNR = 20\,\text{dB}$, $V = 4$).

electromagnetic source models:

- Plane Wave (PW) model characterized by an incident field $\mathbf{E}_{inc}^{v,s}(x,y)\big|_{s=1} = E_0 e^{jkr}\hat{\mathbf{z}}$, $r = x\cos\theta^v + y\sin\theta^v$;
- Isotropic Line (IL) source located at the point ($x_p = r_p\cos\theta^v$, $y_p = r_p\sin\theta^v$), where $r_p = 2.4\lambda_0$ and radiating a field equal to

$$\mathbf{E}_{inc}^{v,s}(x,y)\big|_{s=2} = -I_0\frac{k_0^2}{8\pi f\varepsilon_0}H_0^{(2)}(k_0\rho_p)\hat{\mathbf{z}} \tag{11}$$

  ρ_p being the distance between (x_p, y_p) and (x, y); $I_0 = \sqrt{\frac{8P_0}{\eta k_0}}$, $P_0 = 1\,\frac{mW}{m}$ being the radiated power for unit length and η the intrinsic impedance of the background;
- Directive Line (DL) source modeled by using an expression similar to the Silver's equation [47]

$$\mathbf{E}_{inc}^{v,s}(x,y)\big|_{s=3} = -I_0\frac{k_0^2}{8\pi f\varepsilon_0}H_0^{(2)}(k_0\rho_p)B(\psi)\hat{\mathbf{z}} \tag{12}$$

  where $B(\psi) = \sqrt{\sin^3(\psi)}$ if $0 \le \psi \le \pi$ and $B(\psi) = 0$ otherwise, ψ being the polar angle in a coordinate system centered at (x_p, y_p);
- Composite Source (CS) radiating a field obtained as follows

$$\mathbf{E}_{inc}^{v}(x,y) = \sum_{s=1}^{S}\mathbf{E}_{inc}^{v,s}(x,y) \quad S = 3 \tag{13}$$

Moreover, in order to simulate a real environment, a Gaussian noise characterized by a $SNR = 20\,dB$ has been added to scattered field data.

As far as the IMSA approach is concerned, the following parametric configuration has been used: $K = 2000$, $\delta = 10^{-5}$, $\varsigma = 10^{-6}$, and $K_w = \frac{K}{10}$. Furthermore, in order to test the approach in "worst case" conditions, the background has been chosen as initial guess for the unknown contrast.

To give some quantitative indications on the reconstruction accuracy of the retrieval process, the following error figures will be used

$$\chi_j = \frac{1}{N^{(j)}}\sum_{n=1}^{N^{(j)}}\left\{\frac{\tau(x_n,y_n) - \tau^{ref}(x_n,y_n)}{\tau^{ref}(x_n,y_n)}\right\} \times 100 \tag{14}$$

where $N^{(j)}$ can range over the whole investigation domain ($j \Rightarrow tot$), over the area actually occupied by the scatter ($j \Rightarrow int$), or over the background around the objects ($j \Rightarrow ext$). On the other hand, ξ (center

location error) and Λ (shaping error) will estimate the accuracy of the qualitative imaging

$$\xi = \frac{\sqrt{\left[x_c - x_c^{ref}\right]^2 + \left[y_c - y_c^{ref}\right]^2}}{\lambda_0} \tag{15}$$

$$\Lambda = \left\{ \frac{\left|R - R^{ref}\right|}{R^{ref}} \right\} \times 100 \tag{16}$$

where the super-script "*ref*" refers to the actual profile, R being the radius of the RoI where the scatterer is supposed to be located.

In the first experiment, the inversion process has been carried out by considering simple single-source arrangements (i.e., *PW-model*, *IL-model*, and *DL-model*) in order to generate some reference cases for evaluating the effectiveness of the MS approach. By applying the IMSA methodology, the D_I has been partitioned (at the first step of the multi-scaling procedure) in $N = 49$ square sub-domains and the obtained results are shown in Figs. 2(b)–(d) with a grey-level representation[§]. As it can be observed, whatever the simple single-source illumination, the retrieved profiles slightly relate to the actual stratified configuration (Fig. 2). Although no-artifacts are present in the reconstruction and the scatterer is roughly located in the correct area of the investigation domain ($\xi \simeq 0.30$ — Table 1), significant errors turn out both in the shaping and in the detection of the two-layer structure as confirmed by the values of the error figures ($\Lambda > 38.0$ and $\chi_j > 21.0$, $j \Rightarrow tot, int, ext$ — Table 1). Moreover, it is worth noting that the best reconstruction is yielded with the simplest source-model (i.e., the plane-wave illumination). Such a result seems to indicate that, in general, there is not a direct relation between complexity of the illumination modeling and achievable reconstruction accuracy.

Table 1. Dielectric profile reconstruction ($\tau_{ext} = 2.0$, $\tau_{int} = 0.5$; $SNR = 20\,\text{dB}$) — Error figures when $V = 4$.

	χ_{tot}	χ_{int}	χ_{ext}	ξ	Λ
IMSA-DL	26.12	35.52	25.19	0.31	39.11
IMSA-IL	25.6	38.38	24.37	0.37	38.67
IMSA-PW	22.07	23.90	21.89	0.35	43.56
IMSA-CS	29.00	51.77	26.73	1.38	67.11
IMSA-MS	11.33	18.41	10.63	0.13	24.00

§ Please note that the black pixel in the lower right border is used for reference and the dashed line indicates the region occupied by the actual scatterer.

To further confirm such a concept, let us consider the retrieved profile when the so-called composite source (CS) is used. In this situation, the electromagnetic source has been obtained as the superposition of the incident fields radiated by the SS-models. The obtained image [Fig. 2(e)] turns out to be even worse than that of the SS-models with an increasing of the qualitative ($\xi = 1.38$ and $\Lambda = 67.11$) as well as quantitative ($\chi_{int} = 51.77$) errors.

By leaving aside the study of the optimal illumination for the problem at hand (whose analysis is beyond the scope of this paper), the IMSA-MS strategy has been taken into account. The reconstruction turns out significantly improved both pictorially [Fig. 2(f)] and in terms of error figures. In particular, it should be observed that the layered structure is clearly distinguishable and the scatterer turns out better localized ($\xi^{(DL)} \simeq 2.4\,\xi^{(MS)}$) and dimensioned ($\Lambda^{(MS)} = 24.00$ vs. $\Lambda^{(IL)} = 38.67$).

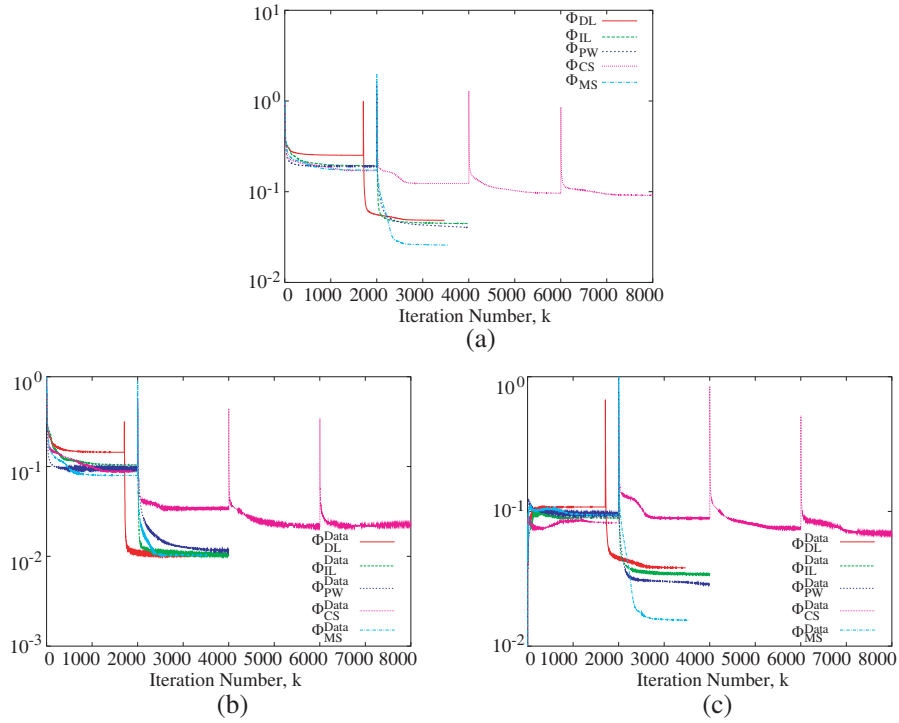

Figure 3. Dielectric profile reconstruction ($\tau_{ext} = 2.0$, $\tau_{int} = 0.5$, $SNR = 20\,\text{dB}$, $V = 4$). Behavior of the (a) cost function and related, (b) data, and (c) state terms during the iterative process.

Table 2. Dielectric profile reconstruction ($\tau_{ext} = 2.0$, $\tau_{int} = 0.5$; $SNR = 20\,\mathrm{dB}$) — Error figures when $V = 6$.

	χ_{tot}	χ_{int}	χ_{ext}	ξ	Λ
IMSA-DL	5.98	19.67	4.60	0.05	7.10
IMSA-IL	4.10	23.51	2.13	0.02	4.44
IMSA-PW	5.26	25.13	3.30	0.03	1.60
IMSA-CS	5.91	28.31	3.70	0.04	3.60
IMSA-MS	1.26	13.72	0.02	0.02	3.56

Such a result has been achieved by minimizing the cost function (8) as shown in Fig. 3 where the two terms of the functional are given, as well. When the IMSA-MS method is adopted, the minimization reaches a lower value of the cost function thus allowing a more accurate data-inversion.

In the second experiment, the number of views has been increased from $V = 4$ to $V = 6$ in order to assess the effectiveness of the proposed approach in different illumination conditions. As expected, the reconstructions significantly improve (Fig. 4 and Table 2) with a decrease of the error values (ξ, Λ, and χ_{tot}) of about one order in magnitude compared to the $V = 4$ condition (as an example, $\chi_{tot}^{(MS)}\Big|_{V=4} / \chi_{tot}^{(MS)}\Big|_{V=6} \simeq 9.0$). Whatever strategy, the two-layers profile is clearly detected. However, the IMSA-MS further confirms its potentialities by overcoming other SS-strategies ($\chi_{tot}^{(IL)} \simeq 3.25\,\chi_{tot}^{(MS)}$, $\chi_{int}^{(DL)} \simeq 1.50\,\chi_{int}^{(MS)}$, and $\frac{\chi_{ext}^{(DL)}}{\chi_{ext}^{(MS)}} \simeq 1.0 \times 10^2$) and by achieving a faithful image of the original profile [Fig. 4(e)].

Although such experiments indicate that it proves conveniently in terms of achievable resolution accuracy to use the multi-source strategy, it is needed to evaluate the arising computational burden, as well. Towards this end, Fig. 5 gives an overview of the computational scenario by resuming the two experiments with different illuminations. More in detail, the following representative parameters are shown: the number of problem unknowns U [Fig. 5(a)], the number of steps of the IMSA I_{opt} [Fig. 5(b)], the total number of iterations of the minimization procedure $K_{tot} = \sum_{i=1}^{I_{opt}} k_{conv}^{(i)}$ ($k_{conv}^{(i)}$ being the number of iterations needed to achieve the "convergence" at the i-th step of the multi-scaling process) [Fig. 5(c)], and the iteration time t_k [Fig. 5(d)]. As it can be observed, even though the number of unknowns triples, the multi-scaling process is terminated at the same number

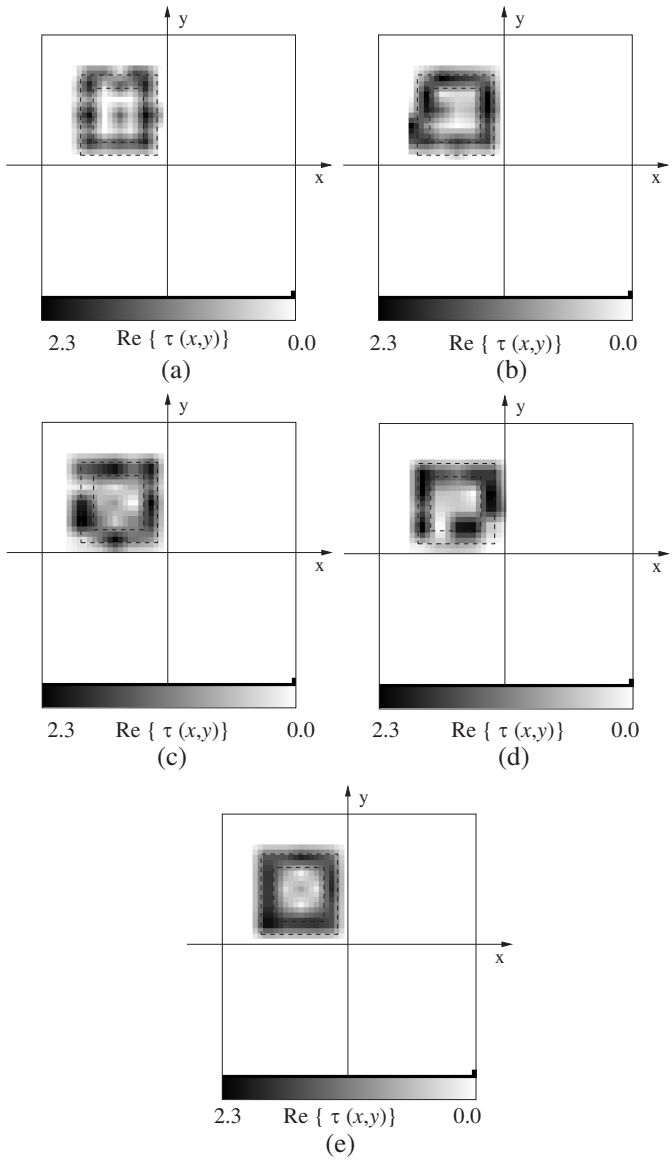

Figure 4. Dielectric profile reconstruction ($\tau_{ext} = 2.0$, $\tau_{int} = 0.5$, $SNR = 20\,\mathrm{dB}$, $V = 6$). Reconstructed dielectric distribution by using (b) *IMSA-PW*, (c) *IMSA-IL*, (d) *IMSA-DL*, (e) *IMSA-CS*, and (f) *IMSA-MS*.

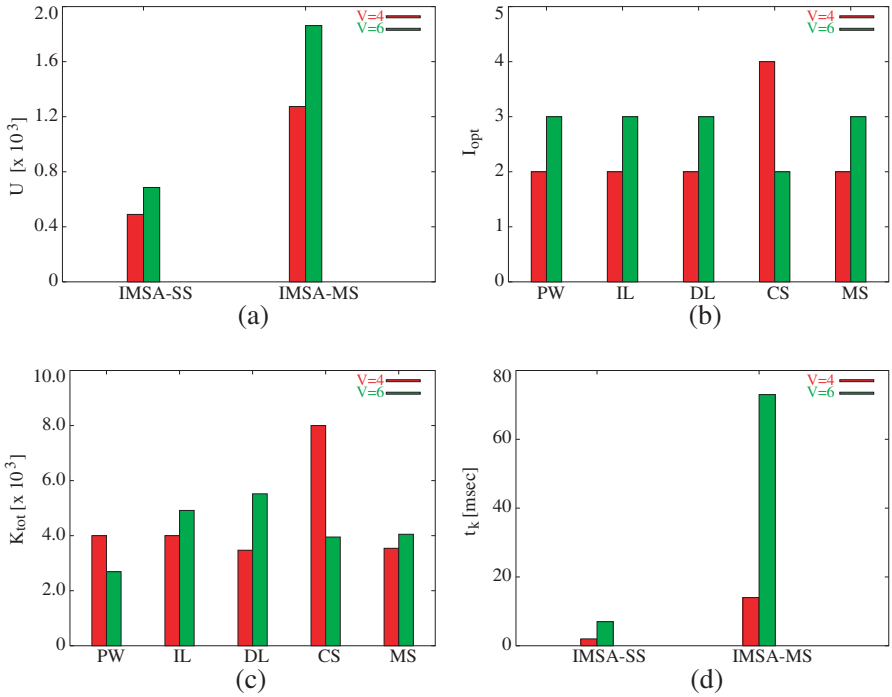

Figure 5. Dielectric profile reconstruction ($\tau_{ext} = 2.0$, $\tau_{int} = 0.5$, $SNR = 20\,\text{dB}$). Evaluation of the computational burden/complexity: (a) Problem dimension U, (b) number of IMSA steps I_{opt}, (c) total number of iterations K_{tot}, and (d) iteration time t_k $[msec]$.

of steps ($I_{opt}^{(MS)}\Big|_{V=4} = 2$ and $I_{opt}^{(MS)}\Big|_{V=6} = 3$) as for SS-approaches and, generally, with a lower K_{tot}. Therefore, the expected increasing of the iteration-time does not impact so-significantly and it does not prevent the feasibility of the proposed approach. As a matter of fact, the problem at hand is still computationally tractable (thanks to the integration with the IMSA). Moreover, the trade-off between increased computational costs and enhanced reconstruction accuracy seems to be in favor of the IMSA-MS.

The advantages of the MS over SS-strategies in terms of reconstruction accuracy are further pointed out and emphasized when more complex geometries are at hand. In these situations, the enhancement allowed by the proposed strategy turns out to be even more significant than in "*Test Case 1*". To show such a behavior, the second test (*Test Case 2*) deals with the asymmetric profile shown

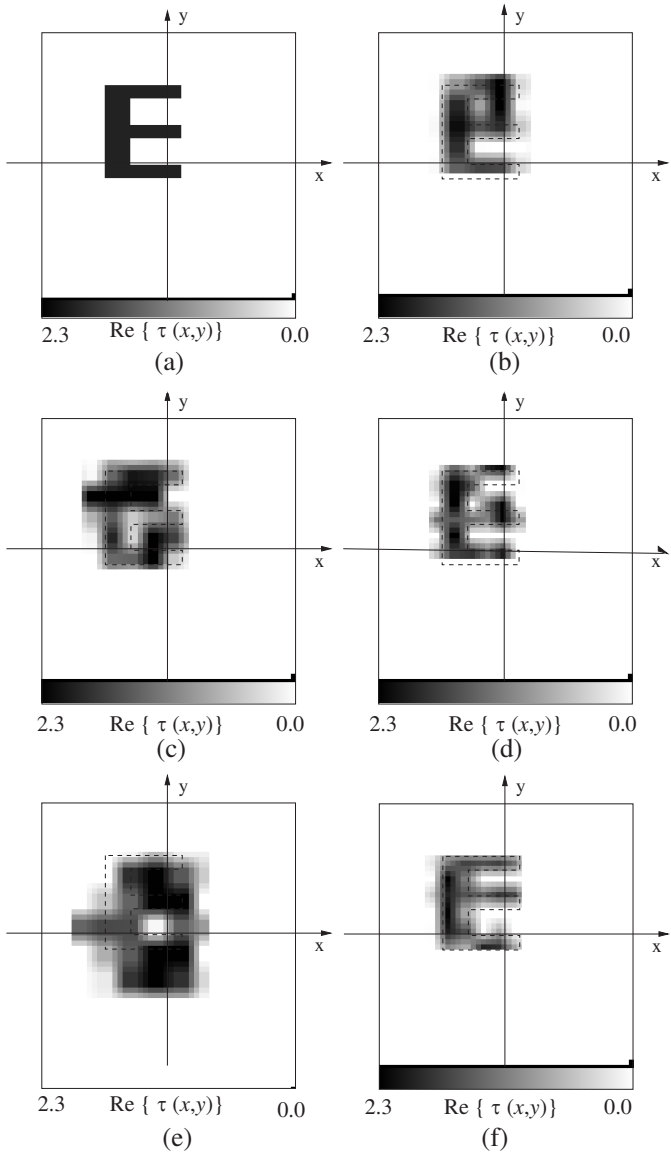

Figure 6. Complex dielectric profile ($\tau = 2.0$). (a) Reference distribution. Reconstructed dielectric distribution by using (b) *IMSA-PW*, (c) *IMSA-IL*, (d) *IMSA-DL*, (e) *IMSA-CS*, and (f) *IMSA-MS* ($SNR = 20\,\mathrm{dB}$, $V = 6$).

in Fig. 6(a) and characterized by the following dielectric/geometric parameters: $x_c^{ref} = -0.392\,\lambda_0$, $y_c^{ref} = 0.374\,\lambda_0$, $H_{ext} = 1.05\,\lambda_0$, $t_{arm} = 0.15\,\lambda_0$ (thickness of the arms), $d_{arm} = 0.3\lambda_0$ (distance between arms), and $\tau = 2.0$. The scatterer has been successively illuminated by $V = 6$ directions and a noise of $SNR = 20\,\text{dB}$ has been added to the field data. Unfortunately, the IMSA-IL and the IMSA-CS single-source approaches completely fail in reconstructing the shape of the object under test as it can be seen in Figs. 6(c) and (e), respectively, and quantified in Table 3 (e.g., $\chi_{tot}^{(IL)} = 17.67$ and $\chi_{tot}^{(CS)} = 28.47$; $\Lambda^{(IL)} = 11.60$ and $\Lambda^{(CS)} = 65.0$). As far as the IMSA-PW is concerned, the upper arm is lost while the lower one is correctly detected [Fig. 6(b)]. A "breaking" improvement of the image quality arises when the DL-SS illumination is used [Fig. 6(d)]. In such a case, while the scatterer cannot be identified exactly, the retrieval procedure converges to a structure that occupies a large subset of the true object. However, once again the MS strategy [Fig. 6(f)] allows a better reconstruction ($\chi_{tot}^{(DL)} \simeq 1.7\,\chi_{tot}^{(MS)}$, $\chi_{ext}^{(DL)} \simeq 2.0\,\chi_{tot}^{(MS)}$, and $\xi^{(DL)} \simeq 10\,\xi^{(MS)}$). As a matter of fact, the final reconstruction is essentially identical to that one would achieve with the lack of edge-preserving or binary-regularization techniques [48].

Table 3. Complex dielectric profile ($\tau = 2.0$; $SNR = 20\,\text{dB}$, $V = 6$) — Error figures.

	χ_{tot}	χ_{int}	χ_{ext}	ξ	Λ
IMSA-DL	6.37	13.31	5.90	0.08	3.20
IMSA-IL	17.67	20.95	17.44	0.03	11.60
IMSA-PW	6.50	15.82	5.87	0.13	4.0
IMSA-CS	28.47	23.33	28.83	0.08	65.0
IMSA-MS	3.80	16.33	2.99	0.007	2.40

4. CONCLUSION

A nonlinear multisource strategy for the quantitative imaging of unknown scatterers has been presented dealing with two-dimensional geometries. The approach is aimed at increasing the reconstruction accuracy by enlarging the non-redundant information on the scenario under test through an effective exploitation of different electromagnetic interactions between various probing sources and scatterers. The method has been developed by exploiting and extending the multiview

technique to the case of multisource data through the definition of a suitable cost function to be minimized. Notwithstanding its simplicity, the proposed strategy turned out to be effective in recovering various permittivity profiles from simple shapes up to complex configurations. Moreover, it is expected to enhance the performance of standard single-source approaches when dealing with multiple scatterers. As far as the increment of the computational load is concerned, the integration of the multisource approach into an iterative multi-scaling procedure allowed a sustainable overhead. Moreover, it is worth pointing out that the different source contributions can be processed almost in an independent fashion so that a parallel implementation [49] would be very easy. This task together with the use of more effective optimization techniques [37] will be matter of future researches.

APPENDIX A.

In order to apply the conjugate-gradient minimization procedure, the computation of $\nabla\Phi_{MS}$ given by

$$\nabla\Phi_{MS} = \nabla\Phi_{MS}^{Data} + \nabla\Phi_{MS}^{State} \tag{A1}$$

is derived. The computation of partial derivatives of Φ_{MS}^{Data} and Φ_{MS}^{State} with respect to the variables $\mathrm{Re}\{\tau_n\}$, $\mathrm{Im}\{\tau_n\}$, $\mathrm{Re}\{E_n^{v,s}\}$, and $\mathrm{Im}\{E_n^{v,s}\}$ is required (where Re{ } and Im{ } indicate real and imaginary part, respectively).

Firstly, let us give some preliminary definitions useful for the following

$$\Psi_{Data}^{(s)}\{\tau_n, E_n^{v,s}\} = E_{scatt}^{s,v}(x_m^v, y_m^v) - \Theta_{Data}^{(s)}\{\tau_n, E_n^{v,s}\} \tag{A2}$$

$$\Psi_{State}^{(s)}\{\tau_n, E_n^{v,s}\} = E_{inc}^{s,v}(x_n, y_n) - \Theta_{State}^{(s)}\{\tau_n, E_n^{v,s}\} \tag{A3}$$

where $\Theta_{Data}^{(s)}\{\tau_n, E_n^{v,s}\} = \sum_{n=1}^{N} \tau_n E_n^{v,s} G_{2D}^v(x_m^v, y_m^v | x_n, y_n)$ and $\Theta_{State}^{(s)}\{\tau_n, E_n^{v,s}\} = E_n^{v,s} - \sum_{p=1}^{N} \tau_p E_p^{v,s} G_{2D}^v(x_n, y_n | x_p, y_p)$.

As far as the "*Data*" term is concerned, by means of simple mathematical manipulations, the following expressions for the partial derivatives of $\Psi_{Data}^{(s)}$ are obtained

$$\frac{\partial\Psi_{Data}^{(s)}}{\partial\{\mathrm{Re}(\tau_n)\}} = \frac{\partial \mathrm{Re}\left\{\Theta_{Data}^{(s)}\right\}}{\partial\{\mathrm{Re}(\tau_n)\}} - j\frac{\partial \mathrm{Im}\left\{\Theta_{Data}^{(s)}\right\}}{\partial\{\mathrm{Re}(\tau_n)\}} \tag{A4}$$

$$\frac{\partial\Psi_{Data}^{(s)}}{\partial\{\mathrm{Im}(\tau_n)\}} = -\frac{\partial \mathrm{Re}\left\{\Theta_{Data}^{(s)}\right\}}{\partial\{\mathrm{Im}(\tau_n)\}} - j\frac{\partial \mathrm{Im}\left\{\Theta_{Data}^{(s)}\right\}}{\partial\{\mathrm{Im}(\tau_n)\}} \tag{A5}$$

where

$$\frac{\partial\left\{\mathrm{Re}\left(\Theta_{Data}^{(s)}\right)\right\}}{\partial\left\{\mathrm{Re}\left(\tau_n\right)\right\}} = \frac{\pi}{2}k_0a_nJ_1\left(k_0a_n\right)\left[\mathrm{Re}\left\{E_n^{v,s}\right\}Y_0\left(k_0\rho_{mn}\right) - \mathrm{Im}\left\{E_n^{v,s}\right\}J_0\left(k_0\rho_{mn}\right)\right] \tag{A6}$$

$$\frac{\partial\left\{\mathrm{Re}\left(\Theta_{Data}^{(s)}\right)\right\}}{\partial\left\{\mathrm{Im}\left(\tau_n\right)\right\}} = -\frac{\pi}{2}k_0a_nJ_1\left(k_0a_n\right)\left[\mathrm{Im}\left\{E_n^{v,s}\right\}Y_0\left(k_0\rho_{mn}\right) + \mathrm{Re}\left\{E_n^{v,s}\right\}J_0\left(k_0\rho_{mn}\right)\right] \tag{A7}$$

$$\frac{\partial\left\{\mathrm{Im}\left(\Theta_{Data}^{(s)}\right)\right\}}{\partial\left\{\mathrm{Re}\left(\tau_n\right)\right\}} = \frac{\pi}{2}k_0a_nJ_1\left(k_0a_n\right)\left[\mathrm{Re}\left\{E_n^{v,s}\right\}J_0\left(k_0\rho_{mn}\right) + \mathrm{Im}\left\{E_n^{v,s}\right\}Y_0\left(k_0\rho_{mn}\right)\right] \tag{A8}$$

$$\frac{\partial\left\{\mathrm{Im}\left(\Theta_{Data}^{(s)}\right)\right\}}{\partial\left\{\mathrm{Im}\left(\tau_n\right)\right\}} = \frac{\pi}{2}k_0a_nJ_1\left(k_0a_n\right)\left[-\mathrm{Im}\left\{E_n^{v,s}\right\}J_0\left(k_0\rho_{mn}\right) + \mathrm{Re}\left\{E_n^{v,s}\right\}Y_0\left(k_0\rho_{mn}\right)\right] \tag{A9}$$

and

$$\frac{\partial\Psi_{Data}^{(s)}}{\partial\left\{\mathrm{Re}\left(E_n^{v,s}\right)\right\}} = -\frac{\partial\mathrm{Re}\left\{\Theta_{Data}^{(s)}\left\{\tau_n, E_n^{v,s}\right\}\right\}}{\partial\left\{\mathrm{Re}\left(E_n^{v,s}\right)\right\}} - j\frac{\partial\mathrm{Im}\left\{\Theta_{Data}^{(s)}\left\{\tau_n, E_n^{v,s}\right\}\right\}}{\partial\left\{\mathrm{Re}\left(E_n^{v,s}\right)\right\}} \tag{A10}$$

$$\frac{\partial\Psi_{Data}^{(s)}}{\partial\left\{\mathrm{Im}\left(E_n^{v,s}\right)\right\}} = -\frac{\partial\mathrm{Re}\left\{\Theta_{Data}^{(s)}\left\{\tau_n, E_n^{v,s}\right\}\right\}}{\partial\left\{\mathrm{Im}\left(\tau_n\right)\right\}} - j\frac{\partial\mathrm{Im}\left\{\Theta_{Data}^{(s)}\left\{\tau_n, E_n^{v,s}\right\}\right\}}{\partial\left\{\mathrm{Im}\left(\tau_n\right)\right\}} \tag{A11}$$

where

$$\frac{\partial\left\{\mathrm{Re}\left(\Theta_{Data}^{(s)}\right)\right\}}{\partial\left\{\mathrm{Re}\left(E_n^{v,s}\right)\right\}} = \frac{\pi}{2}k_0a_nJ_1\left(k_0a_n\right)\left[\frac{\sigma_n}{2\pi f\varepsilon_0}J_0\left(k_0\rho_{mn}\right) + \left(\varepsilon_{r_n}-1\right)Y_0\left(k_0\rho_{mn}\right)\right] \tag{A12}$$

$$\frac{\partial\left\{\mathrm{Re}\left(\Theta_{Data}^{(s)}\right)\right\}}{\partial\left\{\mathrm{Im}\left(E_n^{v,s}\right)\right\}} = \frac{\pi}{2}k_0a_nJ_1\left(k_0a_n\right)\left[\frac{\sigma_n}{2\pi f\varepsilon_0}Y_0\left(k_0\rho_{mn}\right) - \left(\varepsilon_{r_n}-1\right)J_0\left(k_0\rho_{mn}\right)\right] \tag{A13}$$

$$\frac{\partial\left\{\mathrm{Im}\left(\Theta_{Data}^{(s)}\right)\right\}}{\partial\left\{\mathrm{Re}\left(E_n^{v,s}\right)\right\}} = \frac{\pi}{2}k_0 a_n J_1\left(k_0 a_n\right)\left[\left(\varepsilon_{r_n}-1\right)J_0\left(k_0\rho_{mn}\right) - \frac{\sigma_n}{2\pi f\varepsilon_0}Y_0\left(k_0\rho_{mn}\right)\right] \quad \text{(A14)}$$

$$\frac{\partial\left\{\mathrm{Im}\left(\Theta_{Data}^{(s)}\right)\right\}}{\partial\left\{\mathrm{Im}\left(E_n^{v,s}\right)\right\}} = \frac{\pi}{2}k_0 a_n J_1\left(k_0 a_n\right)\left[\frac{\sigma_n}{2\pi f\varepsilon_0}Y_0\left(k_0\rho_{mn}\right) - \left(\varepsilon_{r_n}-1\right)J_0\left(k_0\rho_{mn}\right)\right] \quad \text{(A15)}$$

Accordingly, the partial derivatives of Φ_{MS}^{Data} are given by

$$\frac{\partial\Phi_{MS}^{Data}}{\partial\left\{\mathrm{Re}\left(\tau_n\right)\right\}} = \frac{1}{\sum_{s=1}^{S}\sum_{v=1}^{V}\sum_{m=1}^{M}\left|E_{scatt}^{s,v}(x_m^v,y_m^v)\right|^2}\left\{\sum_{m=1}^{M}\left[2\mathrm{Re}\left\{\Psi_{Data}^{(s)}\left\{\tau_n,E_n^{v,s}\right\}\right\}\frac{\partial\mathrm{Re}\left\{\Psi_{Data}^{(s)}\right\}}{\partial\left\{\mathrm{Re}\left(\tau_n\right)\right\}} + 2\mathrm{Im}\left\{\Psi_{Data}^{(s)}\left\{\tau_n,E_n^{v,s}\right\}\right\}\frac{\partial\mathrm{Im}\left\{\Psi_{Data}^{(s)}\right\}}{\partial\left\{\mathrm{Re}\left(\tau_n\right)\right\}}\right]\right\} \quad \text{(A16)}$$

$$\frac{\partial\Phi_{MS}^{Data}}{\partial\left\{\mathrm{Im}\left(\tau_n\right)\right\}} = \frac{1}{\sum_{s=1}^{S}\sum_{v=1}^{V}\sum_{m=1}^{M}\left|E_{scatt}^{s,v}(x_m^v,y_m^v)\right|^2}\left\{\sum_{m=1}^{M}\left[2\mathrm{Re}\left\{\Psi_{Data}^{(s)}\left\{\tau_n,E_n^{v,s}\right\}\right\}\frac{\partial\mathrm{Re}\left\{\Psi_{Data}^{(s)}\right\}}{\partial\left\{\mathrm{Im}\left(\tau_n\right)\right\}} + 2\mathrm{Im}\left\{\Psi_{Data}^{(s)}\left\{\tau_n,E_n^{v,s}\right\}\right\}\frac{\partial\mathrm{Im}\left\{\Psi_{Data}^{(s)}\right\}}{\partial\left\{\mathrm{Im}\left(\tau_n\right)\right\}}\right]\right\} \quad \text{(A17)}$$

$$\frac{\partial\Phi_{MS}^{Data}}{\partial\left\{\mathrm{Re}\left(E_n^{v,s}\right)\right\}} = \frac{1}{\sum_{s=1}^{S}\sum_{v=1}^{V}\sum_{m=1}^{M}\left|E_{scatt}^{s,v}(x_m^v,y_m^v)\right|^2}\left\{\sum_{m=1}^{M}\left[2\mathrm{Re}\left\{\Psi_{Data}^{(s)}\left\{\tau_n,E_n^{v,s}\right\}\right\}\frac{\partial\mathrm{Re}\left\{\Psi_{Data}^{(s)}\right\}}{\partial\left\{\mathrm{Re}\left(E_n^{v,s}\right)\right\}} + 2\mathrm{Im}\left\{\Psi_{Data}^{(s)}\left\{\tau_n,E_n^{v,s}\right\}\right\}\frac{\partial\mathrm{Im}\left\{\Psi_{Data}^{(s)}\right\}}{\partial\left\{\mathrm{Re}\left(E_n^{v,s}\right)\right\}}\right]\right\} \quad \text{(A18)}$$

$$\frac{\partial \Phi_{MS}^{Data}}{\partial \left\{ \mathrm{Im}\left(E_n^{v,s} \right) \right\}} = \frac{1}{\sum_{s=1}^{S} \sum_{v=1}^{V} \sum_{m=1}^{M} \left| E_{scatt}^{s,v}(x_m^v, y_m^v) \right|^2} \left\{ \sum_{m=1}^{M} \left[2\mathrm{Re}\left\{ \Psi_{Data}^{(s)} \left\{ \tau_n, E_n^{v,s} \right\} \right\} \frac{\partial \mathrm{Re}\left\{ \Psi_{Data}^{(s)} \right\}}{\partial \left\{ \mathrm{Im}\left(E_n^{v,s} \right) \right\}} + 2\mathrm{Im}\left\{ \Psi_{Data}^{(s)} \left\{ \tau_n, E_n^{v,s} \right\} \right\} \frac{\partial \mathrm{Im}\left\{ \Psi_{Data}^{(s)} \right\}}{\partial \left\{ \mathrm{Im}\left(E_n^{v,s} \right) \right\}} \right] \right\} \quad \text{(A19)}$$

Analogously, it is possible to evaluate the partial derivatives of Φ_{MS}^{State}, which are given by

$$\frac{\partial \Phi_{MS}^{State}}{\partial \{ \mathrm{Re}\left(\tau_n \right) \}} = \frac{1}{\sum_{s=1}^{S} \sum_{v=1}^{V} \sum_{p=1}^{N} \left| E_{inc}^{s,v}(x_p, y_p) \right|^2} \left\{ \sum_{p=1}^{N} \pi k_o a_n \left[\mathrm{Re}\left\{ \Psi_{State}^{(s)} \left\{ \tau_p, E_p^{v,s} \right\} \right\} \left\{ \mathrm{Im}\left\{ E_p^{v,s} \right\} I_{np} - \mathrm{Re}\left\{ E_p^{v,s} \right\} R_{np} \right\} - \mathrm{Im}\left\{ \Psi_{State}^{(s)} \left\{ \tau_p, E_p^{v,s} \right\} \right\} \left\{ \mathrm{Re}\left\{ E_p^{v,s} \right\} I_{np} - \mathrm{Re}\left\{ E_p^{v,s} \right\} R_{np} \right\} \right] \right\} \quad \text{(A20)}$$

$$\frac{\partial \Phi_{MS}^{State}}{\partial \{ \mathrm{Im}\left(\tau_n \right) \}} = \frac{1}{\sum_{s=1}^{S} \sum_{v=1}^{V} \sum_{p=1}^{N} \left| E_{inc}^{s,v}(x_p, y_p) \right|^2} \left\{ \sum_{p=1}^{N} \pi k_o \rho_n \left[\mathrm{Re}\left\{ \Psi_{State}^{(s)} \left\{ \tau_p, E_p^{v,s} \right\} \right\} \left\{ \mathrm{Im}\left\{ E_p^{v,s} \right\} R_{np} + \mathrm{Re}\left\{ E_p^{v,s} \right\} I_{np} \right\} + \mathrm{Im}\left\{ \Psi_{State}^{(s)} \left\{ \tau_p, E_p^{v,s} \right\} \right\} \left\{ \mathrm{Im}\left\{ E_p^{v,s} \right\} I_{np} - \mathrm{Re}\left\{ E_p^{v,s} \right\} R_{np} \right\} \right] \right\} \quad \text{(A21)}$$

$$\frac{\partial \Phi_{MS}^{State}}{\partial \{ \mathrm{Re}(E_n^{v,s}) \}} = \frac{1}{\sum_{s=1}^{S} \sum_{v=1}^{V} \sum_{p=1}^{N} \left| E_{inc}^{s,v}(x_p, y_p) \right|^2} \left\{ \sum_{p=1}^{N} \pi k_o a_n \left[\mathrm{Re}\left\{ \Psi_{State}^{(s)} \left\{ \tau_p, E_p^{v,s} \right\} \right\} \left\{ -\frac{2\delta_{np}}{\pi k_0 a_n} - \left(\varepsilon_{r_p} - 1 \right) R_{np} - \frac{\sigma_p}{2\pi f \varepsilon_0} I_{np} \right\} + \mathrm{Im}\left\{ \Psi_{State}^{(s)} \left\{ \tau_p, E_p^{v,s} \right\} \right\} \left\{ \left(\varepsilon_{r_p} - 1 \right) I_{np} + \frac{\sigma_p}{2\pi f \varepsilon_0} R_{np} \right\} \right] \right\} \quad \text{(A22)}$$

$$\frac{\partial \Phi_{MS}^{State}}{\partial \{ \mathrm{Im}(E_n^{v,s}) \}} = \frac{1}{\sum_{s=1}^{S} \sum_{v=1}^{V} \sum_{p=1}^{N} \left| E_{inc}^{s,v}(x_p, y_p) \right|^2} \left\{ \sum_{p=1}^{N} \pi k_o a_n \left[\mathrm{Re}\left\{ \Psi_{State}^{(s)} \right.\right.$$

$$\left\{\tau_p, E_p^{v,s}\right\}\Bigg\}\left\{-\frac{\sigma_p}{2\pi f\varepsilon_0}R_{np}+\left(\varepsilon_{r_p}-1\right)I_{np}\right\}-\mathrm{Im}\left\{\Psi_{State}^{(s)}\left\{\tau_p, E_p^{v,s}\right\}\right\}$$
$$\left\{\frac{2\delta_{np}}{\pi k_0 a_n}+\left(\varepsilon_{r_p}-1\right)R_{np}+\frac{\sigma_p}{2\pi f\varepsilon_0}I_{np}\right\}\Big]\Bigg\} \tag{A23}$$

where

$$R_{np} = \begin{cases} J_1\left(k_0 a_n\right) Y_0\left(k_0\rho_{np}\right) & \text{if } n=p \\ Y_1\left(k_0 a_n\right) \quad \text{if } n\neq p \end{cases} \tag{A24}$$

$$I_{np} = \begin{cases} J_1\left(k_0 a_n\right) J_0\left(k_0\rho_{np}\right) & \text{if } n=p \\ J_1\left(k_0 a_n\right) - \frac{4}{\pi k_0 a_n} \quad \text{if } n\neq p \end{cases} \tag{A25}$$

and $\delta_{np}=1$ if $n=p$, $\delta_{np}=0$ otherwise.

Finally, the array

$$\nabla\Phi_{MS}=\left\{\left[\nabla\Phi_{MS}\right]_{\tau_n}, \left[\nabla\Phi_{MS}\right]_{E_n^{v,s}}; n=1,\ldots,N; v=1,\ldots,V; s=1,\ldots,S\right\}$$

can be computed as

$$\left[\nabla\Phi_{MS}\right]_{\tau_n} = \left[\frac{\partial\Phi_{MS}^{Data}}{\partial\left\{\mathrm{Re}\left(\tau_n\right)\right\}}+\frac{\partial\Phi_{MS}^{State}}{\partial\left\{\mathrm{Re}\left(\tau_n\right)\right\}}\right] + j\left[\frac{\partial\Phi_{MS}^{Data}}{\partial\left\{\mathrm{Im}\left(\tau_n\right)\right\}}+\frac{\partial\Phi_{MS}^{State}}{\partial\left\{\mathrm{Im}\left(\tau_n\right)\right\}}\right] \tag{A26}$$

$$\left[\nabla\Phi_{MS}\right]_{E_n^{v,s}} = \left[\frac{\partial\Phi_{MS}^{Data}}{\partial\left\{\mathrm{Re}\left(E_n^{v,s}\right)\right\}}+\frac{\partial\Phi_{MS}^{State}}{\partial\left\{\mathrm{Re}\left(E_n^{v,s}\right)\right\}}\right] + j\left[\frac{\partial\Phi_{MS}^{Data}}{\partial\left\{\mathrm{Im}\left(E_n^{v,s}\right)\right\}}+\frac{\partial\Phi_{MS}^{State}}{\partial\left\{\mathrm{Im}\left(E_n^{v,s}\right)\right\}}\right] \tag{A27}$$

REFERENCES

1. Abubakar, A., P. M. Van den Berg, and J. T. Fokkema, "Time-lapse TM-polarization electromagnetic imaging," *Subsurf. Sensing Tech. Applic.,* Vol. 4, 117–135, 2003.
2. Yu, Y., T. Yu, and L. Carin, "Three-dimensional inverse scattering of a dielectric target embedded in a lossy half-space," *IEEE Trans. Geosci. Remote Sensing,* Vol. 42, 957–973, 2004.
3. Hoole, S. R. H., S. Subramaniam, R. Saldanha, J.-L. Coulomb, and J.-C. Sabonnadiere, "Inverse problem methodology and finite elements in the identifications of cracks, sources, materials, and their geometry in inaccessible locations," *IEEE Trans. Magn.*, Vol. 27, 3433–3443, 1991.
4. Bolomey, J. C., *Frontiers in Industrial Process Tomography*, Engineering Foundation, 1995.

5. Bolomey, J. C., "Recent European developments in active microwave imaging for industrial, scientific, and medical applications," *IEEE Trans. Microwave Theory Tech.*, Vol. 37, 2109–2117, 1991.
6. Louis, K., "Medical imaging: State of the art and future development," *Inverse Problems*, Vol. 8, 709–738, 1992.
7. Caorsi, S., A. Massa, M. Pastorino, and A. Rosani, "Microwave medical imaging: Potentialities and limitations of a stochastic optimization technique," *IEEE Trans. Microwave Theory Tech.*, Vol. 52, 1909–1916, 2004.
8. Colton, D. and R. Kress, *Inverse Acoustics and Electromagnetic Scattering Theory*, Springer-Verlag, Berlin, Germany, 1992.
9. Bertero, M. and P. Boccacci, *Introduction to Inverse Problem in Imaging*, IoP Publishing, Philadelphia, 1998.
10. Denisov, A. M., *Elements of Theory of Inverse Problems*, VSP, Utrecht, The Netherlands, 1999.
11. Belkebir, K., J. M. Elissalt, J. M. Geffrin, and C. Pichot, "Newton-Kantorovich and modified gradient — Inversion algorithms applied to Ipswich data," *IEEE Antennas Propag. Mag.*, Vol. 38, 41–43, 1996.
12. Franchois, A. and C. Pichot, "Microwave imaging-complex permittivity reconstruction with a Levenberg-Marquardt method," *IEEE Trans. Antennas Propagat.*, Vol. 45, 203–215, 1997.
13. Pastorino, M., A. Massa, and S. Caorsi, "A microwave inverse scattering technique for image reconstruction based on a genetic algorithm," *IEEE Trans. Instrum. Meas.*, Vol. 49, No. 3, 573–578, Jun. 2000.
14. Van den Berg, P. M. and A. Abubakar, "Contrast source inversion method: State of art," *Progress In Electromagnetics Research*, PIER 34, 189–218, 2001.
15. Caorsi, S., M. Donelli, A. Lommi, and A. Massa, "Location and imaging of two-dimensional scatterers by using a particle swarm algorithm," *Journal Electromagnetic Waves Applications*, Vol. 18, 481–494, 2004.
16. Caorsi, S., G. L. Gragnani, and M. Pastorino, "An approach to microwave imaging using a multiview moment method solution for a two-dimensional infinite cylinder," *IEEE Trans. Microwave Theory Tech.*, Vol. 39, 1062–1067, 1991.
17. Bucci, O. M. and T. Isernia, "Electromagnetic inverse scattering: retrievable information and measurements strategies," *Radio Science*, 2123–2138, 1997.

18. Belkebir, K., R. Kleinman, and C. Pichot, "Microwave imaging — Location and shape reconstruction from multifrequency scattering data," *IEEE Trans. Microwave Theory Tech.*, Vol. 45, 469–475, 1997.
19. Bucci, O. M., L. Crocco, T. Isernia, and V. Pascazio, "Inverse scattering problems with multifrequency data: Reconstruction capabilities and solution strategies," *IEEE Trans. Geosci. Remote Sensing*, Vol. 38, 1749–1756, 2000.
20. Franceschini, D., M. Donelli, R. Azaro, and A. Massa, "Dealing with multifrequency scattering data through the IMSA," *IEEE Trans. Antennas Propagat.*, Vol. 55, 2412–2417, 2007.
21. Zhang, W., L. Li, and F. Li, "Multifrequency imaging from intensity-only data using the phaseless data distorted Rytov iterative method," *IEEE Trans. Antennas Propagat.*, Vol. 57, 290–295, 2009.
22. Chew, W. C. and J.-H. Lin, "A frequency-hopping approach for microwave imaging of large inhomogeneous bodies," *IEEE Microwave Guided Wave Lett.*, Vol. 5, 439–441, 1995.
23. Caorsi, S., M. Donelli, D. Franceschini, and A. Massa, "A new methodology based on an iterative multi-scaling for microwave imaging," *IEEE Trans. Microwave Theory Tech.*, Vol. 51, 1162–1173, 2003.
24. Donelli, M., D. Franceschini, P. Rocca, and A. Massa, "Three-dimensional microwave imaging problems solved through an efficient multi-scaling particle swarm optimization," *IEEE Trans. Geosci. Remote Sens.*, Vol. 47, 1467–1481, 2009.
25. Franceschini, D., M. Donelli, G. Franceschini, and A. Massa, "Iterative image reconstruction of two-dimensional scatterers illuminated by TE waves," *IEEE Trans. Microwave Theory Techn.*, Vol. 54, 1484–1494, Apr. 2006.
26. Kaas, M., W. Rieger, C. Huber, G. Lehner, and W. M. Rucker, "Improvement of inverse scattering results by combining TM- and TE-polarized probing waves using an iterative adaptation technique," *IEEE Trans. Magn.*, Vol. 35, 1574–1577, 1999.
27. Chou, C.-P. and Y.-W. Kiang, "Inverse scattering of dielectric cylinders by a cascaded TE-TM method," *IEEE Trans. Microwave Theory Techn.*, Vol. 47, 1923–1930, 1999.
28. Poli, L. and P. Rocca, "Exploitation of TE-TM scattering data for microwave imaging through the multi-scaling reconstruction strategy," *Progress In Electromagnetics Research*, PIER 99, 245–260, 2009.

29. Isernia, T., V. Pascazio, and R. Pierri, "On the local minima in a tomographic imaging technique," *IEEE Trans. Geosci. Remote Sensing,* Vol. 39, 1596–1607, 2001.
30. Jones, D. S., *The Theory of Electromagnetism*, Pergamon Press, Oxford, UK 1964.
31. Richmond, J. H., "Scattering by a dielectric cylinder of arbitrary cross section shape," *IEEE Trans. Antennas Propagat.*, Vol. 13, 334–341, 1965.
32. Caorsi, S., A. Massa, and M. Pastorino, "Numerical assessment concerning a focused microwave diagnostic method for medical applications," *IEEE Trans. Antennas Propagat.*, Vol. 48, 1815–1830, 2000.
33. Kohn, R. V. and A. McKenney, "Numerical implementation of a variational method for electrical impedance tomography," *Inverse Problems,* Vol. 6, 389–414, 1990.
34. Caorsi, S., A. Massa, and M. Pastorino, "A computational technique based on a real-coded genetic algorithm for microwave imaging purposes," *IEEE Trans. Geosci. Remote Sens.*, Vol. 38, 1697–1708, 2000.
35. Caorsi, S., A. Massa, M. Pastorino, and A. Randazzo, "Electromagnetic detection of dielectric scatterers using phaseless synthetic and real data and the memetic algorithm," *IEEE Trans. Geosci. Remote Sens.*, Vol. 41, 2745–2753, 2003.
36. Donelli, M. and A. Massa, "A computational approach based on a particle swarm optimizer for microwave imaging of two-dimensional dielectric scatterers," *IEEE Trans. Microwave Theory Techn.*, Vol. 53, 1761–1776, 2004.
37. Rocca, P., M. Benedetti, M. Donelli, D. Franceschini, and A. Massa, "Evolutionary optimization as applied to inverse problems," *Inverse Problems — 25th Year Special Issue of Inverse Problems, Invited Topical Review*, Vol. 25, 2009.
38. Van den Berg, P. M. and R. E. Kleinman, "A contrast source inversion method," *Inverse Problems,* Vol. 13, 1607–1620, 1997.
39. Caorsi, S., M. Donelli, and A. Massa, "Detection, location and imaging of multiple scatterers by means of the iterative multiscaling method," *IEEE Trans. Microwave Theory Techn.*, Vol. 52, 1217–1228, 2004.
40. Caorsi, S., M. Donelli, and A. Massa, "Analysis of the stability and robustness of the iterative multi-scaling approach for microwave imaging applications," *Radioscience*, Vol. 39, 2004.
41. Franceschini, G., D. Franceschini, and A. Massa, "Full-vectorial

three-dimensional microwave imaging through the iterative multi-scaling strategy — A preliminary assessment," *IEEE Geosci. Remote Sens. Lett.*, Vol. 2, 428–432, 2005.

42. Donelli, M., G. Franceschini, A. Martini, and A. Massa, "An integrated multi-scaling strategy based on a particle swarm algorithm for inverse scattering problems," *IEEE Trans. Geosci. Remote Sens.*, Vol. 44, 298–312, 2006.
43. Benedetti, M., D. Lesselier, M. Lambert, and A. Massa, "A multi-resolution technique based on shape optimization for the reconstruction of homogeneous dielectric objects," *Inverse Problems*, Vol. 25, 1–26, 2009.
44. Donelli, M., D. Franceschini, G. Franceschini, and A. Massa, "Effective exploitation of multi-view data through the iterative multi-scaling method — An experimental assessment," *Progress In Electromagnetics Research*, PIER 54, 137–154, 2005.
45. Franceschini, G., M. Donelli, R. Azaro, and A. Massa, "Inversion of phaseless total field data using a two-step strategy based on the iterative multi-scaling approach," *IEEE Trans. Geosci. Remote Sens.*, Vol. 44, 3527–3539, 2006.
46. Benedetti, M., A. Casagranda, M. Donelli, and A. Massa, "An adaptive multi- scaling imaging technique based on a fuzzy-logic strategy for dealing with the uncertainty of noisy scattering data," *IEEE Trans. Antennas Propagat.*, Vol. 55, 3265–3278, 2007.
47. Balanis, C. A., *Antenna Theory: Analysis and Design*, Wiley, New York, 1997.
48. Duchène, B., D. Lesselier, and R. E. Kleinman, "Inversion of the 1996 Ipswich data using binary specialization of modified gradient methods," *IEEE Antennas Propag. Mag.*, Vol. 39, 9–12, 1997.
49. Massa, A., D. Franceschini, G. Franceschini, M. Raffetto, M. Pastorino, and M. Donelli, "Parallel GA-based approach for microwave imaging applications," *IEEE Trans. Antennas Propagat.*, Vol. 53, 3118–3127, 2005.